AGU PUBLICATIONS

JGR

Journal of Geophysical Research: Atmospheres

RESEARCH ARTICLE
10.1002/2017JD027512

Key Points:
- The short-term water vapor feedback based on AIRS-MLS observations from 2004 to 2016 is 1.55 ± 0.23 W m^{-2} K^{-1}
- The long-term water vapor feedback inferred from observations is 1.85 ± 0.32 W m^{-2} K^{-1}

Correspondence to:
R. Liu,
liuruncn@163.com

Citation:
Liu, R., Su, H., Liou, K.-N., Jiang, J. H., Gu, Y., Liu, S. C., & Shiu, C.-J. (2018). An assessment of tropospheric water vapor feedback using radiative kernels. *Journal of Geophysical Research: Atmospheres*, *123*, 1499–1509. https://doi.org/10.1002/2017JD027512

Received 26 JUL 2017
Accepted 11 JAN 2018
Accepted article online 17 JAN 2018
Published online 3 FEB 2018

An Assessment of Tropospheric Water Vapor Feedback Using Radiative Kernels

Run Liu[1,2], Hui Su[3], Kuo-Nan Liou[2,4], Jonathan H. Jiang[3], Yu Gu[2,4], Shaw Chen Liu[1], and Chein-Jung Shiu[5]

[1]Institute for Environmental and Climate Research, Jinan University, Guangzhou, China, [2]Joint Institute for Regional Earth System Science and Engineering, University of California, Los Angeles, CA, USA, [3]Jet Propulsion Laboratory, California Institute of Technology, Pasadena, CA, USA, [4]Department of Atmospheric and Oceanic Sciences, University of California, Los Angeles, CA, USA, [5]Research Center for Environmental Changes, Academia Sonica, Taipei, Taiwan

Abstract Water vapor feedbacks on different time scales are investigated using radiative kernels applied to the Atmospheric Infrared Sounder and Microwave Limb Sounder satellite observations, as well as the Coupled Model Intercomparison Project Phase 5 model simulation results. We show that the magnitude of short-term global water vapor feedback based on observed interannual variations from 2004 to 2016 is 1.55 ± 0.23 W m^{-2} K^{-1}, while model-simulated results derived from the Coupled Model Intercomparison Project Phase 5 runs driven by observed sea surface temperature range from 0.99 to 1.75 W m^{-2} K^{-1}, with a multimodel mean of 1.40 W m^{-2} K^{-1}. The long-term water vapor feedbacks derived from the quadrupling of CO_2 runs range from 1.47 to 2.03 W m^{-2} K^{-1}, higher than the short-term counterparts. The systematic difference between short-term and long-term water vapor feedbacks illustrates that care should be taken when inferring long-term feedbacks from interannual variabilities. Also, the magnitudes of the short-term and long-term feedbacks are closely correlated (R = 0.66) across the models, implying that the observed short-term water vapor feedback could be used to constrain the simulated long-term water vapor feedback. Based on satellite observations, the inferred long-term water vapor feedback is about 1.85 ± 0.32 W m^{-2} K^{-1}.

1. Introduction

Water vapor is one of the dominant greenhouse gases in the Earth's atmosphere and poses strong feedbacks on climate change (Sherwood et al., 2010; Soden & Held, 2006). A number of studies based on satellite observations and model simulations (e.g., Dalton & Shell, 2013; Dessler & Sherwood, 2009; Dessler & Wong, 2009; Dessler et al., 2008) have shown that water vapor feedbacks are strongly positive.

Satellite observations can be used to evaluate modeled short-term feedbacks over the same time period. However, it is questionable whether short-term feedbacks are comparable to those on longer time scales. A number of previous studies considered this question by comparing modeled feedbacks over different time scales. For example, Dessler and Wong (2009) suggested that water vapor feedback in response to El Niño–Southern Oscillation is larger than that in response to long-term global warming, due to different patterns of surface warming. Several previous studies have investigated the relationship between climate feedbacks in response to the long-term climate change and the short-term interannual variability (e.g., Colman & Hanson, 2017; Colman & Power, 2010; Zhou et al., 2015). Colman and Power (2010) suggested that the interannual water vapor feedback is only about two thirds the strength of the century-scale transient feedback in a climate model. Colman and Hanson (2017) found that there was a significant relationship between Representative Concentration Pathway (RCP) 8.5 and decadal and interannual climate feedbacks. Takahashi et al. (2016) found the centennial water vapor change per degree of surface warming is systematically higher than that for the interannual variability for 14 climate models that participated in the Coupled Model Intercomparison Project Phase 5 (CMIP5). Gordon et al. (2013) applied a Partial Radiative Perturbation method and linear regressions on the 100 year twentieth century simulations from 14 Coupled Model Intercomparison Project Phase 3 (CMIP3) models to estimate the long-term water vapor feedback. Then they compared the resulting long-term water vapor feedback to the short-term water vapor feedback estimated using only 88 months of model outputs, a data length comparable to that of the then-available satellite observations from the Atmospheric Infrared Sounder (AIRS). They concluded that the short-term water vapor feedback estimates based on at least 25 year satellite record would be within 15% of the long-term water vapor feedback. Using 88 month AIRS observations, they inferred that the long-term water vapor feedback

based on the linear regression of the 100 year water vapor changes onto surface temperature is about 1.9 to 2.8 W m^{-2} K^{-1}. In comparison, Soden and Held (2006) applied the radiative kernel method to the 21st century and 20th century water vapor differences and showed that the centennial water vapor feedback ranges from 1.5 to 2.1 W m^{-2} K^{-1} for the same 14 CMIP3 models. It is clear that the magnitude of water vapor feedback depends on the length of data record, natural variability, and climate change scenarios.

Recently, there has been an increasing interest in separating the rapid response of atmospheric variables to direct CO_2 forcing and the slow response to surface warming when diagnosing climate feedbacks (e.g., Bony et al., 2013; Zelinka et al., 2013). In transient climate simulations such as the 1% annual compound increase of CO_2 experiment or CMIP5 RCP scenarios, changes in radiative forcings, primarily the increase of CO_2, would cause variations in radiative fluxes at the top-of-atmosphere (TOA) even when surface temperature has not increased substantially. Thus, a significant portion of the reduced outgoing longwave radiation at the end of 21st century would be caused by an increased CO_2 concentration regardless of surface warming. Because of the different response time of TOA radiation and surface temperature to CO_2 forcing (Bony et al., 2013), it is necessary to remove the effect of direct CO_2 forcing on TOA radiation when quantifying the magnitude of long-term water vapor feedback, which by definition should include only the radiative perturbations associated with the water vapor change given unit surface warming.

This study extends aforementioned studies to examine the relationship between short-term and long-term water vapor feedbacks, and to provide an updated quantitative estimate of long-term water vapor feedback consistent with contemporary satellite observations. In this study, the short-term water vapor feedback is derived from the interannual variations for a period of 30 years or 12 years (same as the available satellite data) in CMIP5 simulations and satellite observations, while the long-term feedback is derived from the linear regression of water vapor change against surface temperature change in the first 150 years of the CMIP5 model simulations with the CO_2 concentration abruptly increased to 4 times of the preindustrial value and held constant thereafter. This linear regression method applied onto abrupt4 × CO2 runs effectively excludes the fast response to direct CO_2 forcing in total TOA radiation changes (Gregory et al., 2004). Thus, this paper differs from the previous studies in that (1) a greater number of state-of-the-art CMIP5 models are used; (2) a new and cleaner measure of long-term water vapor feedback is considered, eliminating model differences in the fast response to direct CO_2 forcing; and (3) longer satellite observations are used. In the following, we investigated the sensitivity of the results to the length of data record.

Section 2 describes the water vapor feedback analysis method, satellite observations, and model outputs used in the investigation. Section 3 presents observed short-term water vapor feedbacks and a comparison between modeled short-term and long-term water vapor feedbacks, followed by inferring long-term water vapor feedbacks from short-term observations. Conclusions are given in section 4.

2. Methodology and Data

2.1. The Radiative Kernels

Held and Soden (2000) and Soden and Held (2006) introduced the idea of estimating the strength of a climate feedback, λ_x, by decomposing it into two multiplicative terms. The approach is used extensively in climate studies (Jonko et al., 2012; Sanderson & Shell, 2012; Shell et al., 2008; Soden et al., 2008; Yue et al., 2016) and is described as follows:

$$\lambda_X = \sum\nolimits_{x,y,z} \frac{\partial R}{\partial \mathrm{X}(x,y,z)} \frac{\mathrm{d}X(x,y,z)}{\mathrm{d}T_s} \tag{1}$$

where $\partial R/\partial X(x,y,z)$ represents the TOA radiative flux in response to the unit change of a climate variable X, which is a function of space and time and is referred to as the radiative kernel. The term $\mathrm{d}X(x,y,z)/\mathrm{d}T_s$ represents the climate feedback response of X, where T_s denotes the global mean surface temperature. In this study, X is the natural logarithm of atmospheric specific humidity (Q_v) in units of kg kg^{-1}, since the absorption of radiation by water vapor is nearly proportional to the natural logarithm of water vapor amount.

The precalculated National Center for Atmospheric Research (NCAR) Community Atmospheric Model version 3 (CAM3) radiative kernels with a resolution of approximately 2.8° latitude by 2.8° longitude and 17 vertical levels from 1,000 hPa to 100 hPa (Shell et al., 2008) are used in this study. Model and observational fields

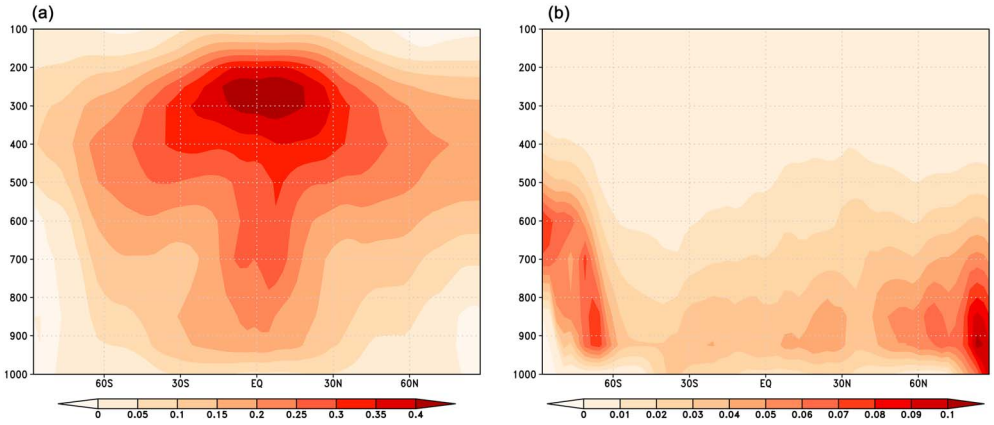

Figure 1. The annual-average (a) longwave and (b) shortwave water vapor kernels (in units of W m^{-2} K^{-1} per 100 hPa) from CAM3.

of $d\ln(Q_v)/dT_s$ are interpolated into this common grid configuration before further processing. Shell et al. (2008) also provide the kernels broken down into longwave (LW) and shortwave (SW) components for water vapor, allowing the separation of computing the LW and SW water vapor feedbacks. A comparison of the kernels generated using different models and different radiation schemes is presented in Soden et al. (2008) and indicates a relative insensitivity of global feedback strength to the kernel functions from different sources; instead, the change in water vapor with respect to T_s largely determines the diversity of the feedback strength. We recognize that the radiative kernels are derived from the present-day CAM3 simulations. It may introduce errors in TOA fluxes when they are applied to the strongly forced abrupt4 × CO2 simulations because of the nonlinearities in radiative calculations (Jonko et al., 2012, 2013). The differences in water vapor feedbacks on short-term and long-term time scales result from both the sensitivity of the water vapor amount to surface warming on different time scales and the changes in the radiative response with climate states (Jonko et al., 2013). Since we use the same set of radiative kernels for both time scales, approximately 14% underestimate of long-term water vapor feedback may be introduced (Jonko et al., 2013).

Table 1
Abbreviation and Name of 20 CMIP5 Models Used in This Study

Mark	Abbreviation	Expanded model name
a	BCC-CSM1-1	Beijing Climate Center Climate System Model version 1.1
b	BCC-CSM1–1-M	Beijing Climate Center Climate System Model version 1.1, moderate resolution
c	BNU-ESM	Beijing Normal University-Earth System Model
d	CNRM-CM5	Centre National de Researches Météorologiques Coupled Global Climate Model, version 5
e	CSIRO-ACCESS1-0	Commonwealth Scientific and Industrial Research Organisation Australian Community Climate and Earth System, version 1.0
f	CSIRO-ACCESS1-3	Commonwealth Scientific and Industrial Research Organisation Australian Community Climate and Earth System, version 1.3
g	CSIRO-Mk3-6-0	Commonwealth Scientific and Industrial Research Organisation Mark, version 3.6.0
h	GFDL-CM3	Geophysical Fluid Dynamics Laboratory Climate Model, version 3
i	GISS-E2-R	Goddard Institute for Space Studies ModelE/Russell
j	INM-CM4	Institute of Numerical Mathematics Coupled Model, version 4.0
k	IPSL-CM5A-LR	L'Institut Pierre-Simon Laplace Coupled Model, version 5, coupled with NEMO, low resolution
l	IPSL-CM5A-MR	L'Institut Pierre-Simon Laplace Coupled Model, version 5, coupled with NEMO, midresolution
m	IPSL-CM5B-LR	L'Institut Pierre-Simon Laplace Coupled Model, version 5, coupled with new atmospheric physic
n	MIROC5	Model for Interdisciplinary Research on Climate, version 5
o	MIROC-ESM	Model for Interdisciplinary Research on Climate Earth System Model
p	MPI-ESM-LR	Max Plank Institute Earth System Model, low resolution
q	MPI-ESM-MR	Max Plank Institute Earth System Model, medium resolution
r	MRI-CGCM3	Meteorological Research Institute Coupled Atmosphere–Ocean General Circulation Model, version 3
s	NCAR-CCSM4	National Center for Atmospheric Research Community Climate System Model, version 4
t	NCC-NorESM1-M	Norwegian Earth System Model, version 1, intermediate resolution

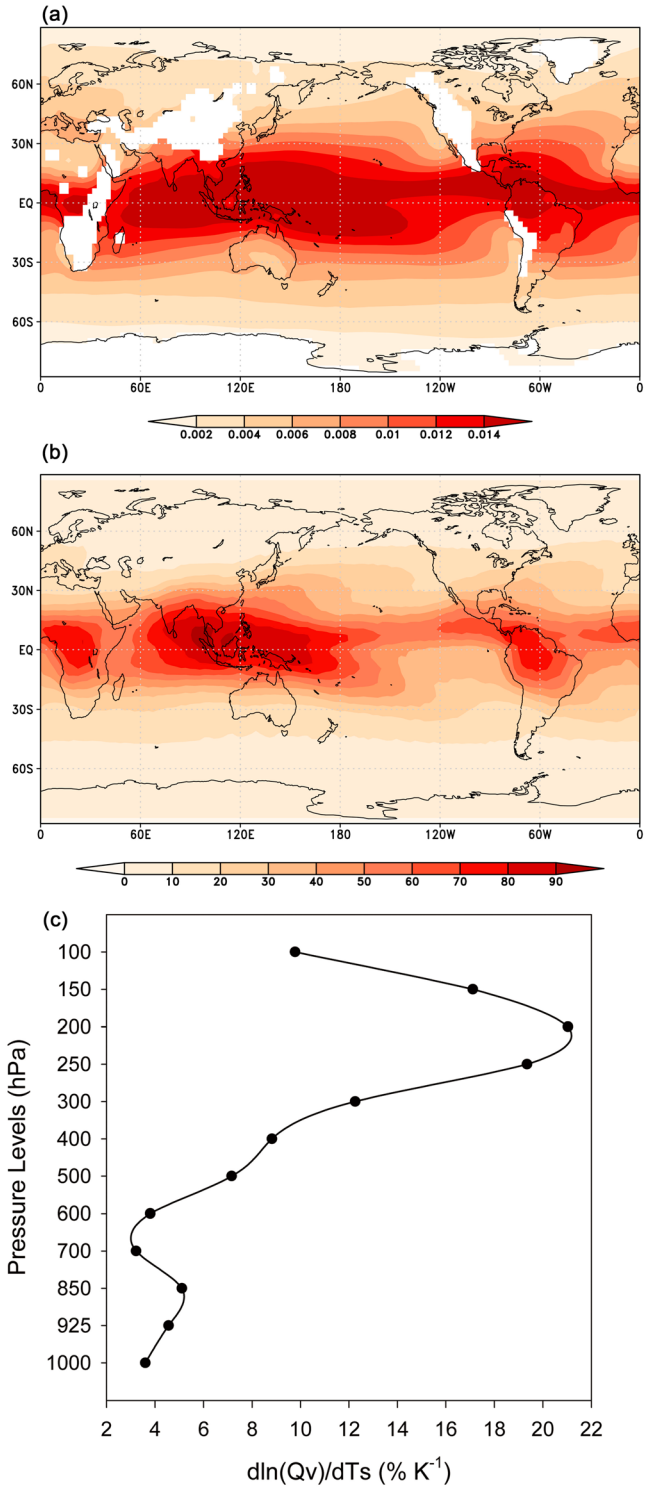

Figure 2. (a) Spatial distribution of Q_v (in units of kg kg^{-1}) at 925 hPa derived from AIRS-MLS observations averaged for August 2004 to July 2016. (b) Same as Figure 2a except for Q_v (in units of 10^{-6} kg kg^{-1}) at 200 hPa. (c) Vertical profile of global mean $d\ln(Q_v)/dT_s$ (in units of % K^{-1}) for AIRS-MLS observations from August 2004 to July 2016.

Figure 1 shows the CAM3 annual mean LW and SW water vapor kernels. Those kernels demonstrate the relative importance of unit change in water vapor with respect to T_s at different latitudes and vertical levels to water vapor feedback strength. The global mean and vertically integrated (from surface to the tropopause) values of LW and SW water vapor kernels are 1.73 and 0.15 W m^{-2} K^{-1}, respectively. Here the unit temperature change corresponds to the Q_v change in kg kg^{-1} per degree of air temperature change under the condition of constant relative humidity at each 100 hPa thick vertical layer. As an increase in water vapor results in a decrease in the outgoing longwave radiation at the TOA, the LW water vapor kernels are mainly positive. The negative kernels near the surface at high latitudes are possibly caused by temperature inversions (Soden et al., 2008). Water vapor also absorbs solar radiation, so the SW kernels are also positive, indicating that an increase in water vapor leads to an increase in net incoming solar radiation. The magnitudes are about a factor of 10 smaller than those of the LW counterpart.

Each model's λ_{Qv} is vertically integrated from the surface to the tropopause and globally averaged to yield the global mean feedback strength. The tropopause height is determined following the approach developed by Soden et al. (2008), which defines the tropopause at 100 hPa at the equator and increasing linearly with latitude to 300 hPa at the poles.

2.2. Water Vapor and Temperature Data

The observed monthly mean tropospheric Q_v and atmospheric temperature (T) are obtained from measurements made by the AIRS (Aumann et al., 2003) on Aqua satellite and Microwave Limb Sounder (MLS) (Waters et al., 2006) on Aura satellite from August 2004 to July 2016, which were lunched in 2002 and 2004, respectively. Aqua and Aura are flying in formation as parts of National Aeronautics and Space Administration's (NASA) A-Train satellites carrying sensors that provide nearly simultaneous and co-located measurements of multiple parameters that can be used for atmospheric process analysis (L'Ecuyer & Jiang, 2010). We have used the AIRS version 6, Level 3 Q_v and T products (Tian et al., 2013) in this study. The data set has a spatial resolution of 50 km but is reported on a 1° × 1° (longitude × latitude) grid. The useful altitude range for the current study is from 1,000 hPa to 300 hPa. For Q_v, the estimated uncertainty is 25% in the tropics, 30% at midlatitudes, and 50% at high latitudes (> 60°N/S). For T, the uncertainty is about 1 K (Fetzer et al., 2005; Jiang et al., 2012; Tian et al., 2013). For Q_v and T at above 300 hPa, MLS version 4.2 Level 2 data are used (Livesey et al., 2017). The useful altitude range of MLS data is at pressure level less than 316 hPa. The measurement uncertainty is ~20% at the tropics and midlatitudes, and ~50% at high latitudes for Q_v (Livesey et al., 2017; Read et al., 2007). We combine AIRS data from 1,000 hPa to 300 hPa and MLS data from 300 hPa to 100 hPa to create the entire tropospheric water vapor profiles as in Jiang et al. (2012). Surface air temperature (T_s) is obtained from Hadley Centre-Climatic Research Unit version 4 data set, a collaborative product of the Met Office Hadley Centre and the Climatic Research Unit at the University of East Anglia (Morice et al., 2012).

To obtain the model simulated short-term $d\ln(Q_v)/dT_s$, we use the CMIP5 Atmospheric Model Intercomparison Project (AMIP) simulations from 1979 to 2008 in which the atmospheric models are driven by the time-varying observed sea surface temperature and sea ice distributions. The interannual $d\ln(Q_v)/dT_s$ is derived from the linear

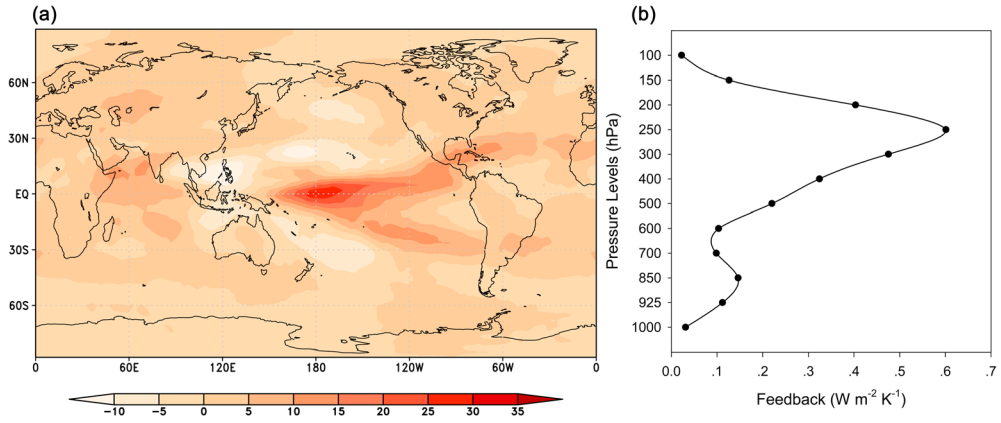

Figure 3. (a) Spatial distribution of water vapor feedbacks (in units of W m^{-2} K^{-1}) derived from AIRS-MLS observations from August 2004 to July 2016. (b) Vertical profile of global mean water vapor feedbacks (in units of W m^{-2} K^{-1}) for AIRS-MLS observations from August 2004 to July 2016.

regression of detrended deseasonalized monthly $\ln(Q_v)$ versus T_s in observations and AMIP model simulations. We use both the full length of AMIP simulations since 1979 and the same length as the observational record (i.e., 12 years) to obtain the interannual water vapor feedbacks in the models in order to quantify the sensitivity of short-term feedback strength data record length used.

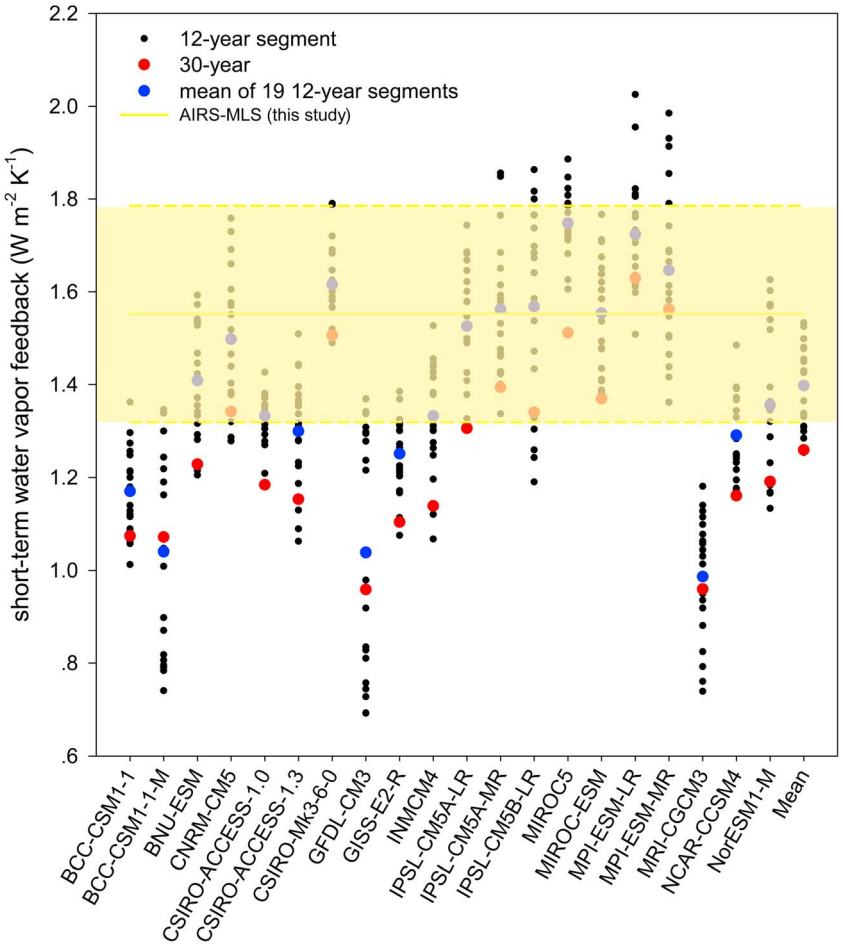

Figure 4. Interannual water vapor feedback (in units of W m^{-2} K^{-1}) derived from CMIP5 AMIP simulations. Red dots are the results for the entire period of 1979–2008, blue dots are the mean of 19 different 12 year segments of the entire record (e.g., 1979–1990, 1980–1991, and 1981–1992), and black dots indicate the results from individual segments. Multimodel means are also shown. The yellow shaded region represents the result from the AIRS-MLS observations during August 2004 to July 2016.

Table 2
Means (Standard Deviations Shown in Parentheses) of Nineteen 12 year, 30 year Short-Term and Long-Term Water Vapor Feedbacks (in Units of W m^{-2} K^{-1}) in 20 CMIP5 Models

Model	Mean of 19 segments (W m^{-2} K^{-1})	30 years (W m^{-2} K^{-1})	Long term (W m^{-2} K^{-1})
BCC-CSM1-1	1.17 (0.09)	1.07	1.47
BCC-CSM1-1-M	1.04 (0.22)	1.07	1.52
BNU-ESM	1.41 (0.12)	1.23	1.55
CNRM-CM5	1.50 (0.15)	1.34	1.56
CSIRO-ACCESS1-0	1.33 (0.05)	1.18	1.63
CSIRO-ACCESS1-3	1.30 (0.12)	1.15	1.61
CSIRO-Mk3-6-0	1.62 (0.09)	1.51	1.67
GFDL-CM3	1.04 (0.26)	0.96	1.69
GISS-E2-R	1.25 (0.08)	1.10	1.67
INM-CM4	1.33 (0.12)	1.14	1.62
IPSL-CM5A-LR	1.53 (0.14)	1.31	1.99
IPSL-CM5A-MR	1.56 (0.15)	1.39	2.03
IPSL-CM5B-LR	1.57 (0.22)	1.34	1.73
MIROC5	1.75 (0.07)	1.51	1.84
MIROC-ESM	1.55 (0.12)	1.37	1.87
MPI-ESM-LR	1.72 (0.13)	1.63	1.88
MPI-ESM-MR	1.65 (0.18)	1.56	1.90
MRI-CGCM3	0.99 (0.14)	0.96	1.57
NCAR-CCSM4	1.29 (0.08)	1.16	1.49
NCC-NorESM1-M	1.36 (0.17)	1.19	1.53
Multimodel mean	1.40 (0.10)	1.26	1.69

The long-term $d\ln(Q_v)/dT_s$ is derived from the linear regression of annual mean $\ln(Q_v)$ versus T_s in the CMIP5 abrupt4 × CO2 simulations, in which the CO_2 concentration is suddenly quadrupled and stays constant throughout. The annual mean Q_v and T_s from piControl runs are subtracted from the corresponding time series in abrupt4 × CO2 runs to minimize the effect of model drifts. A detailed experiment design for CMIP5 simulations can be found in Taylor et al. (2012). These CMIP5 simulation results are downloaded from the CMIP5 data archive (https://esgf-node.llnl.gov/search/cmip5/).

In this study, we analyze water vapor feedbacks from 20 CMIP5 models with humidity and temperature variables available for both short-term and long-term calculations (Table 1). Only the first model ensemble (r1i1p1) run for each model was used in the analysis.

3. Results

3.1. Observed Short-Term Water Vapor Feedback

Figures 2a–2c show the spatial distribution of Q_v at 950 hPa and 200 hPa along with the vertical profile of global mean $d\ln(Q_v)/dT_s$ for AIRS-MLS observations. In both the boundary layer and upper troposphere, large Q_v values are located over the intertropical convergence zone, tropical western Pacific, central Africa, and northern South America. Over the subtropics, Q_v exhibits low values. The spatial pattern of Q_v is primarily controlled by T_s and convective activity. The global mean $d\ln(Q_v)/dT_s$ is about 4.4% K^{-1} in the boundary layer, and it increases with height and peaks at 200 hPa with a value around 21.0% K^{-1}. From 200 hPa to 100 hPa, $d\ln(Q_v)/dT_s$ rapidly decreases to about 9.8% K^{-1}.

Combining CAM3 radiative kernels and the observed changes in water vapor with respect to T_s from AIRS-MLS for the period of August 2004 to July 2016, we derive the observed short-term water vapor feedback. The magnitude of global mean water vapor feedback is 1.55 ± 0.23 W m^{-2} K^{-1}, with the LW contribution of 1.46 ± 0.22 W m^{-2} K^{-1} and the SW counterpart of 0.09 ± 0.01 W m^{-2} K^{-1}. The short-term water vapor feedback derived here is smaller than the value of 2.20 ± 0.40 W m^{-2} K^{-1} estimated by Gordon et al. (2013) using AIRS observation from September 2002 to December 2009. The discrepancy possibly resulted from the different kernels used and different time periods analyzed.

Figure 3a shows the spatial distribution of water vapor feedback integrated over the tropospheric column. The tropics (30°S–30°N) dominates the strength of global mean feedback, because LW water vapor kernels dominate over the deep tropics, and at the same time, water vapor changes per degree of surface

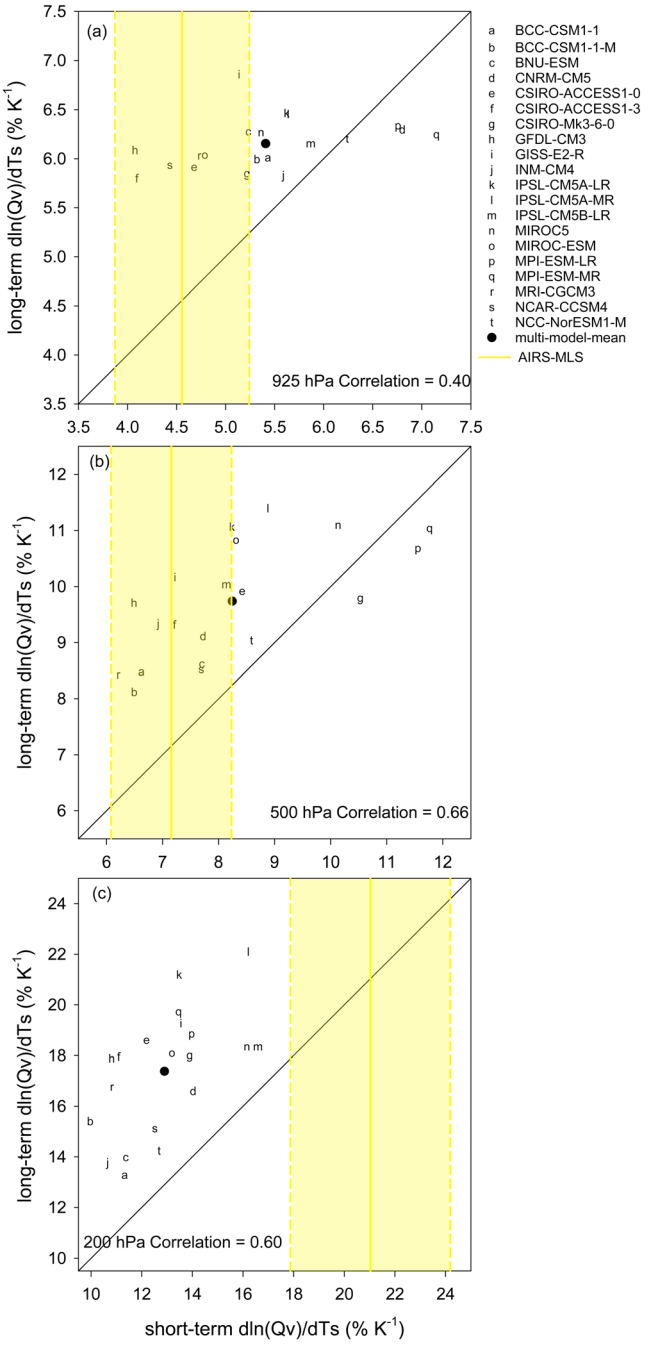

Figure 5. The relationship between the short-term and long-term $d\ln(Q_v)/dT_s$ (in units of % K^{-1}) at different pressure levels: (a) 925 hPa, (b) 500 hPa, and (c) 200 hPa. Each model is represented by a lowercase letter. The yellow shaded regions indicate the short-term $d\ln(Q_v)/dT_s$ derived from AIRS-MLS observations. Multimodel means are marked in solid circles. The correlation coefficients are shown.

warming are strongly enhanced by tropical deep convection in the upper troposphere (Su et al., 2006), resulting in the maximum feedback strength in equatorial regions. Figure 3b displays the globally averaged water vapor feedback at different pressure levels. It is clear that water vapor feedback between 300 hPa and 200 hPa contributes the most, resulting from the relatively larger kernels (Figure 1) and larger water vapor changes per the degree of T_s change (Figure 2c).

3.2. Comparison of Simulated Short-Term and Long-Term Water Vapor Feedbacks

The short-term water vapor feedback for models is first computed using the 30 year interannual variations from January 1979 to December 2008. Then we divide the 30 years record into nineteen 12 year segments (e.g., 1979–1990, 1980–1991, and 1981–1992, etc.) and compute the short-term water vapor feedback for the 19 segments in each model. The choice of 12 year segments is to match the length of available AIRS-MLS water vapor data record. The results are displayed in Figure 4. The water vapor feedbacks derived from 30 year interannual and nineteen 12 year segments show a significant correlation across 20 models with $R > 0.77$. Table 2 compares the mean of nineteen 12 year segments and the 30 year interannual water vapor feedbacks. In general, the multimodel mean of the averaged water vapor feedback strength out of the nineteen 12 year segments (1.40 ± 0.10 W m^{-2} K^{-1}) is slightly greater than the 30 year interannual water vapor feedbacks (1.26 W m^{-2} K^{-1}). The differences across all segments for each model indicate that water vapor changes in response to surface warming are dependent on the time period analyzed since the internal variability dominates the short-term water vapor feedback (Gordon et al., 2013). Hereafter, the average of water vapor feedbacks from the nineteen 12 year segments is referred to as the simulated short-term water vapor feedbacks in order to compare with the same record length from AIRS-MLS observations.

Compared to the AIRS-MLS observed $d\ln(Q_v)/dT_s$, on the short-term time scale, all models underestimate the increase in $\ln(Q_v)$ with T_s at 200 hPa; however, most models overestimate the rate of $d\ln(Q_v)/dT_s$ in the boundary layer (17 out of 20) and at 500 hPa (15 out of 20) (Figure 5). The intermodel spread in the short-term $d\ln(Q_v)/dT_s$ is particularly large at 200 hPa, ranging from 10.0% to 16.6% K^{-1}, indicating a large diversity in the model representation of the effect of deep convection on modulating upper tropospheric moisture (Su et al., 2017).

The model simulated short-term and long-term water vapor changes at three pressure levels (200, 500, and 925 hPa) are displayed in Figure 5, similar to those depicted in Takahashi et al. (2016), whereas centennial changes between RCP4.5 runs and historical runs were used there, different from the results based on arbupt4 × CO2-piControl runs used in this study. In general, the long-term $d\ln(Q_v)/dT_s$ is larger than the short-term $d\ln(Q_v)/dT_s$ for most models, except for MPI-ESM-LR and MPI-ESM-MR at 925 hPa and 500 hPa, and CNRM-CM5 and NCC-NorESM1-M at 925 hPa. These systematic discrepancies between long-term and short-term changes are consistent with previous studies (Colman & Power, 2010; Gordon et al., 2013; Takahashi et al., 2016). Also, the short-term and long-term $d\ln(Q_v)/dT_s$ are positively correlated. The correlations between the short-term and long-term $d\ln(Q_v)/dT_s$ are above 0.40 at all levels.

Short-term and long-term water vapor feedbacks are compared in Figure 6. All of the 20 models (black dots) are located in the upper left side of the 1:1 line, indicating that the simulated short-term water vapor

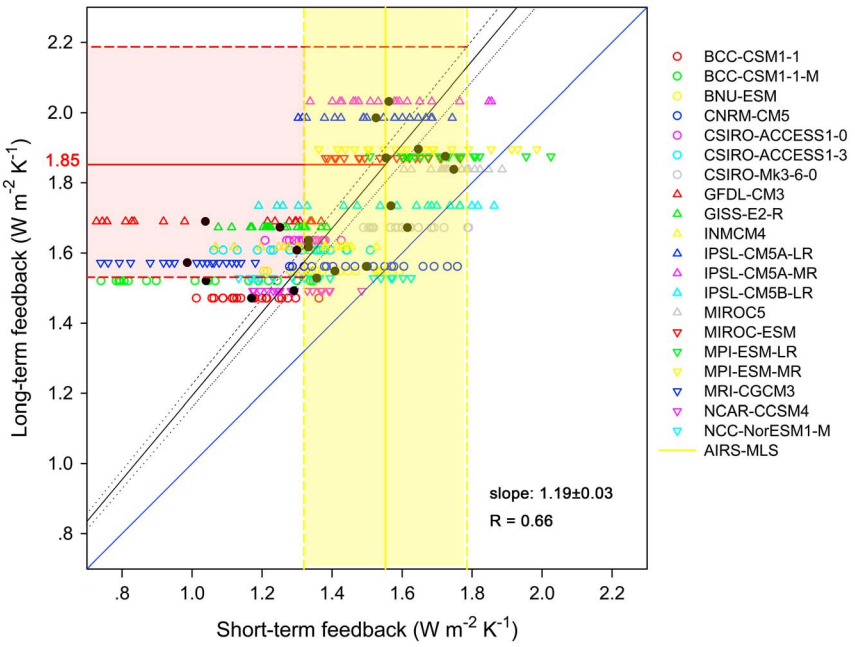

Figure 6. The relationship between short-term and long-term water vapor feedbacks. The nineteen 12 year segments of water vapor feedbacks in each model are marked as colored open symbols. The black solid dots are the means of 12 year feedbacks. The yellow shaded region represents the result from the AIRS-MLS observations during August 2004 to July 2016. The red solid line represents the inferred long-term water vapor feedbacks, and the red shaded region is for uncertainties. The correlation coefficient between 12 year short-term and long-term water vapor feedbacks is also shown.

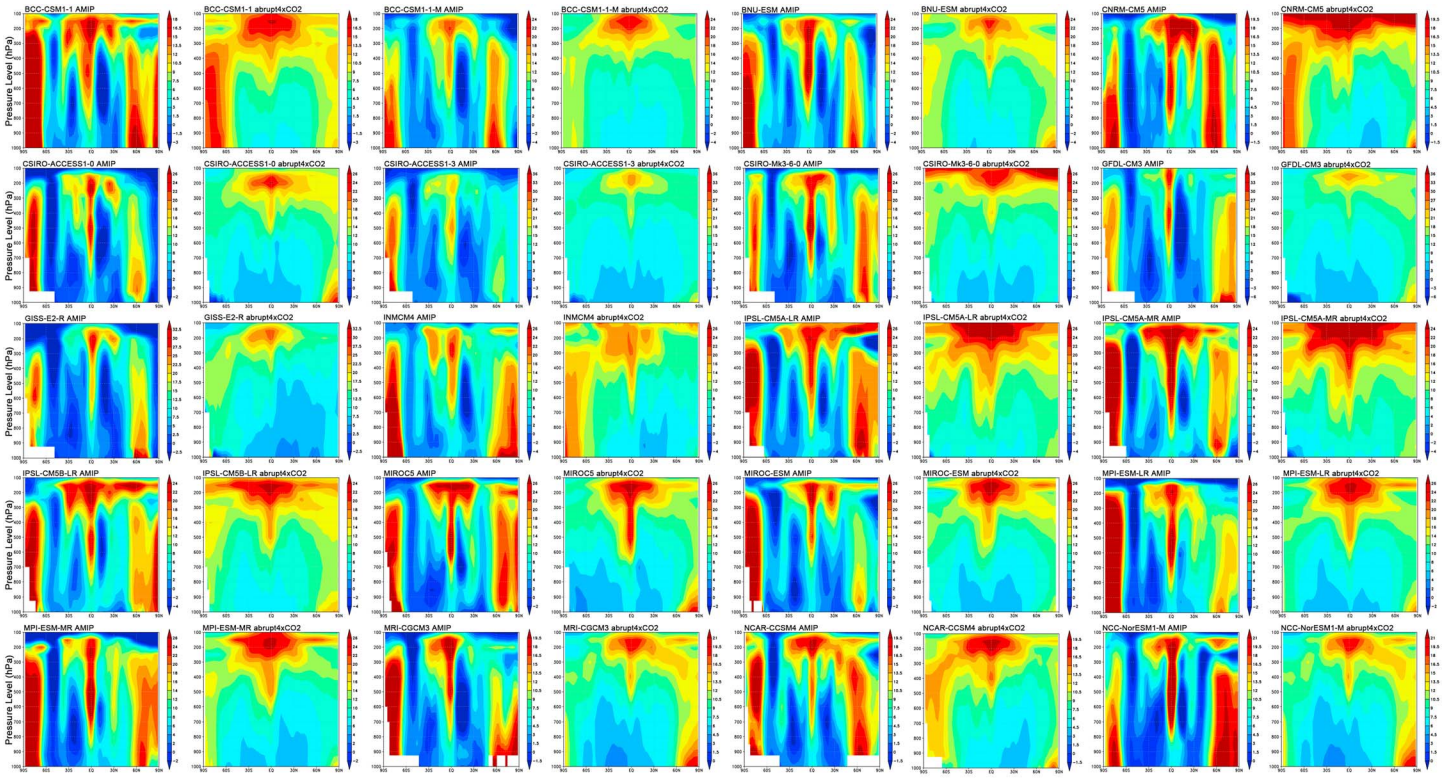

Figure 7. Vertical profiles for zonal mean changes in $\ln(Q_v)$ with respect to T_s (in % K^{-1}) in 20 CMIP5 models used in this study for AMIP (the first, third, fifth, and seventh columns) and abrupt4 × CO2 simulations (the second, fourth, sixth, and eighth columns).

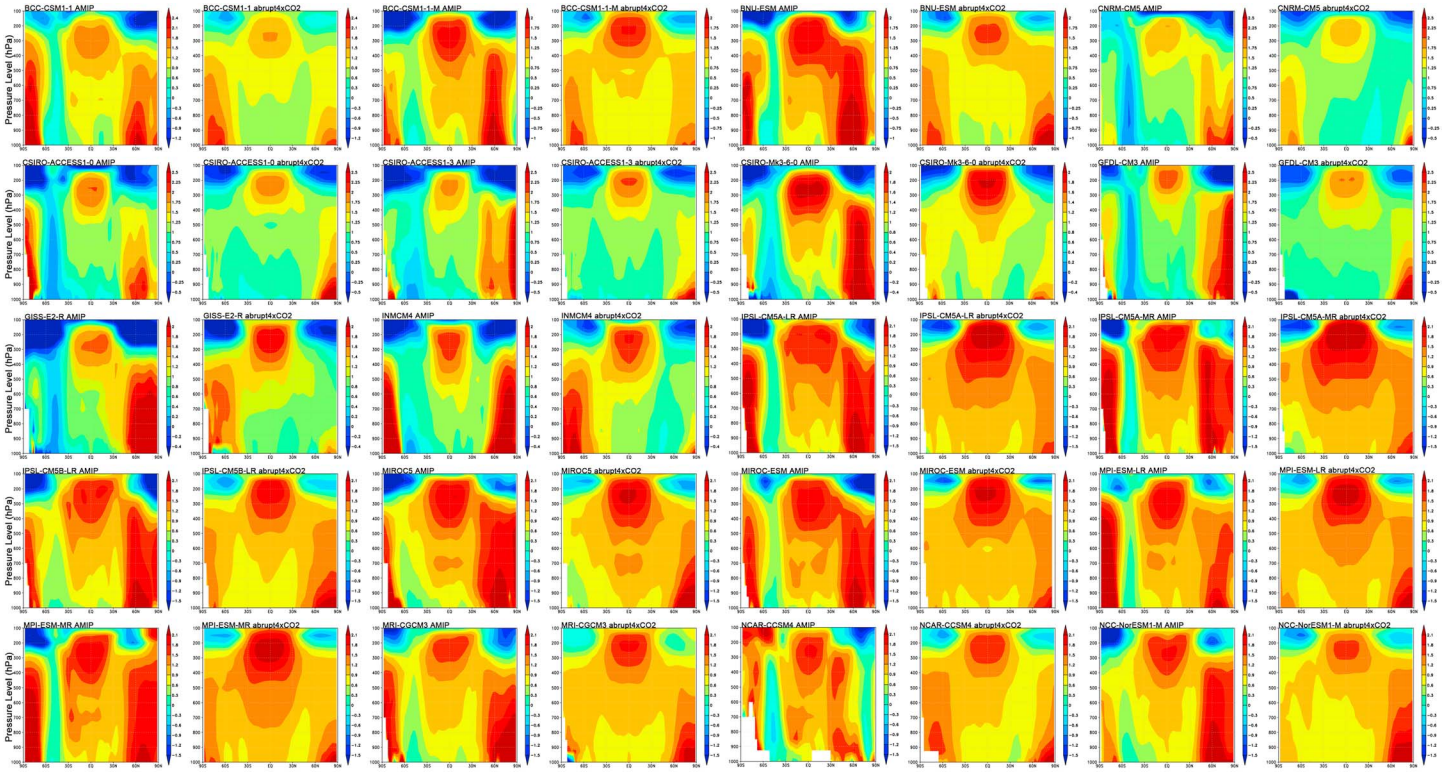

Figure 8. Same as Figure 7 but for changes in air temperature with respect to T_s (in K K^{-1}).

feedback is weaker than the long-term feedback in all models. The systematic differences between short-term and long-term water vapor feedback strengths are resulted from the different latitudinal tropospheric temperature and thus water vapor responses to surface warming on the two time scales. On the short-term time scale, decreases of air temperature and water vapor are found over the midlatitude in the Southern Hemisphere, while a universal warming and moistening are produced on the long-term time scale (Figures 7 and 8). It should be noted that some short-term water vapor feedbacks derived from 12 year segments are greater than the long-term counterparts, implying the time dependence of changes in water vapor with respect to T_s, which is related to the surface warming pattern (Dessler & Wong, 2009).

The simulated short-term water vapor feedbacks range from 0.99 to 1.75 W m^{-2} K^{-1}, with a multimodel mean of 1.40 W m^{-2} K^{-1}. Given the uncertainty of water vapor feedback from AIRS-MLS observations, the models simulate the short-term water vapor feedback well. The long-term water vapor feedback ranges from 1.47 to 2.03 W m^{-2} K^{-1}, with a multimodel mean of 1.69 W m^{-2} K^{-1}, comparable to the estimates presented in previous studies (e.g., Caldwell et al., 2016; Colman & Hanson, 2017; Dessler, 2013; Soden & Held, 2006). It should be noted here that for forcing magnitudes on the order of 2 × CO2, there is a good agreement between modeled TOA fluxes and TOA fluxes derived using radiative kernels (Jonko et al., 2012). However, discrepancies can be found when applying the present-day radiative kernels to abrupt4 × CO2-piControl simulations.

3.3. Inferring Long-Term Water Vapor Feedback From Observations

Figure 6 clearly indicates that short-term water vapor feedbacks are not the same as long-term feedbacks. However, the strong positive correlation between short-term and long-term water vapor feedbacks enables the short satellite observational record to serve as a useful constraint on the long-term water vapor feedback (Dalton & Shell, 2013; Gordon et al., 2013).

Based on the approximately linear relation between short-term and long-term water vapor feedbacks, we attempt to infer the long-term water vapor feedback from satellite observations. The linear regression slope between the long-term and short-term water vapor feedback is 1.19 ± 0.03. According to the linear regression

line between short-term and long-term water vapor feedbacks and the observed short-term water vapor of 1.55 ± 0.23 W m^{-2} K^{-1}, the global mean long-term water vapor feedback that is consistent with the observations is 1.85 ± 0.32 W m^{-2} K^{-1}. The uncertainty of 0.32 W m^{-2} K^{-1} is based on the 95% confidence level of the regression slope and the uncertainty of AIRS-MLS observations shown in Figure 6 (red shaded region). Our estimate of the observationally constrained long-term water vapor feedback is similar to but at the lower end of the value suggested by Gordon et al. (2013) of 1.9 to 2.8 W m^{-2} K^{-1}.

4. Conclusions

This study investigates the short-term water vapor feedback from AIRS-MLS observations during August 2004 to July 2016 using CAM3 radiative kernels and the relationships between simulated short-term and long-term water vapor feedbacks from CMIP5 model simulation results. We have provided an estimate of the long-term water vapor feedback, which is constrained by AIRS-MLS observations. The present analysis of long-term water vapor feedbacks excludes the response of TOA radiation to direct CO_2 forcing and thus more accurately represents the temperature-mediated water vapor feedback strength than previous studies.

Moreover, the present results show that the magnitude of short-term water vapor feedback from AIRS-MLS observation is about 1.55 ± 0.23 W m^{-2} K^{-1}. The short-term water vapor feedbacks derived from CMIP5 AMIP simulations ranging from 0.99 to 1.75 W m^{-2} K^{-1}, with a multimodel mean (1.40 W m^{-2} K^{-1}) slightly smaller than the observed value, while the long-term feedbacks derived from CMIP5 abrupt4 $\times$ CO_2-piControl simulations are greater than the corresponding short-term feedbacks. Interannual variations in the short-term water vapor feedback are dependent on the time period analyzed. Further, we find that a data record length of 30 years does not bring the water vapor feedback strength closer to the long-term water vapor feedback than any of the 12 year segments.

The systematic differences between the long-term water vapor feedback relative to the short-term feedback suggest that the pattern of surface warming and other forcing factors could alter the water vapor response to surface warming on different time scales despite that the response function $d\ln(Q_v)/dT_s$ is largely determined by internal model physics, which lead to the inherent linkage between long-term and short-term variations. In summary, accurate satellite observations of the short-term variabilities are very useful to constrain model simulations, as well as useful to infer long-term climate feedbacks and climate change.

Acknowledgments
This research was supported by the NASA ROSE NEWS and AST programs, and the National Science Foundation under grants AGS-0946315 and AGS-1523296, and the Major Program of the National Natural Science Foundation of China (grant 91644222). Hui Su and Jonathan H. Jiang conducted the work at the Jet Propulsion Laboratory, California Institute of Technology, under contract with NASA. We acknowledge the World Climate Research Programme CMIP5 (http://cmip-pcmdi.llnl.gov/cmip5/) for providing the climate model simulation results. Finally, we are grateful to the three anonymous reviewers for their thoughtful comments, which led to an improved revised manuscript.

References

Aumann, H. H., Chahine, M. T., Gautier, C., Goldberg, M. D., Kalnay, E., McMillin, L. M., … Susskind, J. (2003). AIRS/AMSU/HSB on the Aqua mission: Design, science objectives, data products, and processing systems. *IEEE Transactions on Geoscience and Remote Sensing*, *41*(2), 253–264. https://doi.org/10.1109/TGRS.2002.808356

Bony, S., Bellon, G., Klocke, D., Sherwood, S., Fermepin, S., & Denvil, S. (2013). Robust direct effect of carbon dioxide on tropical circulation and regional precipitation. *Nature Geoscience*, *6*(6), 447–451. https://doi.org/10.1038/ngeo1799

Caldwell, P. M., Zelinka, M. D., Taylor, K. E., & Marvel, K. (2016). Quantifying the sources of inter-model spread in equilibrium climate sensitivity. *Journal of Climate*, *29*(2), 513–524. https://doi.org/10.1175/JCLI-D-15-0352.1

Colman, R. A., & Hanson, L. (2017). On the relative strength of radiative feedbacks under climate variability and change. *Climate Dynamics*, *49*(5-6), 2115–2129. https://doi.org/10.1007/s00382-016-3441-8

Colman, R. A., & Power, S. B. (2010). Atmospheric radiative feedbacks associated with transient climate change and climate variability. *Climate Dynamics*, *34*(7-8), 919–933. https://doi.org/10.1007/s00382-009-0541-8

Dalton, M. M., & Shell, K. M. (2013). Comparison of short-term and long-term radiative feedbacks and variability in twentieth-century global climate model simulations. *Journal of Climate*, *26*(24), 10,051–10,070. https://doi.org/10.1175/JCLI-D-12-00564.1

Dessler, A. E. (2013). Observations of climate feedbacks over 2000–2010 and comparisons to climate models. *Journal of Climate*, *26*(1), 333–342. https://doi.org/10.1175/JCLI-D-11-00640.1

Dessler, A. E., & Sherwood, S. C. (2009). A matter of humidity. *Science*, *323*(5917), 1020–1021. https://doi.org/10.1126/science.1171264

Dessler, A. E., & Wong, S. (2009). Estimates of the water vapor climate feedback during El Niño-Southern Oscillation. *Journal of Climate*, *22*(23), 6404–6412. https://doi.org/10.1175/2009JCLI3052.1

Dessler, A. E., Zhang, Z., & Yang, P. (2008). Water-vapor climate feedback inferred from climate fluctuations, 2003–2008. *Geophysical Research Letters*, *35*, L20704. https://doi.org/10.1029/2008GL035333

Fetzer, E. J., Eldering, A., Fishbein, E. F., Hearty, T., Irion, W. F., & Kahn, B. (2005). *Validation of AIRS/AMSU/HSB core products for data release version 4.0. JPL D-31448* (p. 60). Pasadena, CA: Jet Propulsion Laboratory.

Gordon, N. D., Jonko, A. K., Forster, P. M., & Shell, K. M. (2013). An observationally based constraint on the water-vapor feedback. *Journal of Geophysical Research: Atmospheres*, *118*, 12,435–12,443. https://doi.org/10.1002/2013JD020184

Gregory, J. M., Ingram, W. J., Palmer, M. A., Jones, G. S., Stott, P. A., Thorpe, R. B., … Williams, K. D. (2004). A new method for diagnosing radiative forcing and climate sensitivity. *Geophysical Research Letters*, *31*, L03205. https://doi.org/10.1029/2003GL018747

Held, I. M., & Soden, B. J. (2000). Water vapor feedback and global warming. *Annual Review of Energy and the Environment*, *25*(1), 441–475. https://doi.org/10.1146/annurev.energy.25.1.441

Jiang, J. H., Hui, S., Zhai, C., Perun, V. S., Del Genio, A., Nazarenko, L., … Stephens, G. R. (2012). Evaluation of cloud and water vapor simulations in CMIP5 climate models using NASA A-Train satellite observations. *Journal of Geophysical Research*, *117*, D14105. https://doi.org/10.1029/2011JD017237

Jonko, A. K., Shell, K. M., Sanderson, B. M., & Danabasoglu, G. (2012). Climate feedbacks in CCSM3 under changing CO_2 forcing. Part I: Adapting the linear radiative kernel technique to feedback calculations for a broad range of forcings. *Journal of Climate*, *25*(15), 5260–5272. https://doi.org/10.1175/JCLI-D-11-00524.1

Jonko, A. K., Shell, K. M., Sanderson, B. M., & Danabasoglu, G. (2013). Climate feedbacks in CCSM3 and changing CO_2 forcing. Part II: Variation of climate feedbacks and sensitivity with forcing. *Journal of Climate*, *26*(9), 2784–2795. https://doi.org/10.1175/JCLI-D-12-00479.1

L'Ecuyer, T. S., & Jiang, J. H. (2010). Touring the atmosphere aboard the A-Train. *Physics Today*, *63*(7), 36–41. https://doi.org/10.1063/1.3463626

Livesey, N. J., Read, W. G., Wagner, P. A., Froidevaux, L, Lambert, A., Manney, G. L., … Martinez, E. (2017). Earth Observing System (EOS) Aura Microwave Limb Sounder (MLS) version 4.2x level 2 data quality and description document. Pasadena, CA: JPL D-33509 Rev. C, Jet Propulsion Laboratory.

Morice, G. P., Kennedy, J. J., Rayner, N. A., & Jones, P. D. (2012). Quantifying uncertainties in global and regional temperature change using an ensemble of observational estimates: The HadCRUT4 dataset. *Journal of Geophysical Research*, *117*, D08101. https://doi.org/10.1029/2011JD017187

Read, W. G., Lambert, A., Bacmeister, J., Cofield, R. E., Christensen, L. E., Cuddy, D. T., … Wu, D. L. (2007). Aura Microwave Limb Sounder upper tropospheric and lower stratospheric H_2O and relative humidity with respect to ice validation. *Journal of Geophysical Research*, *112*, D24S35. https://doi.org/10.1029/2007JD008752

Sanderson, B. M., & Shell, K. M. (2012). Model-specific radiative kernels for calculating cloud and noncloud climate feedbacks. *Journal of Climate*, *25*(21), 7607–7624. https://doi.org/10.1175/JCLI-D-11-00726.1

Shell, K. M., Kiehl, J. T., & Shields, C. A. (2008). Using the radiative kernel technique to calculate climate feedbacks in NCAR'S community atmospheric model. *Journal of Climate*, *21*(10), 2269–2282. https://doi.org/10.1175/2007JCLI2044.1

Sherwood, S. C., Roca, R., Weckwerth, T. M., & Andronova, N. G. (2010). Tropospheric water vapor, convection, and climate. *Reviews of Geophysics*, *48*, RG2001. https://doi.org/10.1029/2009RG000301

Soden, B. J., & Held, I. M. (2006). An assessment of climate feedbacks in coupled ocean-atmosphere models. *Journal of Climate*, *19*(14), 3354–3360. https://doi.org/10.1175/JCLI3799.1

Soden, B. J., Colman, R., Shell, K. M., Kiehl, J. T., & Shields, C. A. (2008). Quantifying climate feedbacks using radiative kernels. *Journal of Climate*, *21*(14), 3504–3520. https://doi.org/10.1175/2007JCLI2110.1

Su, H., Read, W. G., Jiang, J. H., Waters, J. W., Wu, D. L., & Fetzer, E. J. (2006). Enhanced positive water vapor feedback associated with tropical deep convection: New evidence from Aura MLS. *Geophysical Research Letters*, *33*, L05709. https://doi.org/10.1029/2005GL025505

Su, H., Jiang, J. H., Neelin, J. D., Shen, T. J., Zhai, C., Yue, Q., … Yung, Y. L. (2017). Tightening of tropical ascent and high clouds key to precipitation change in a warmer climate. *Nature Communications*, *8*, 15771. https://doi.org/10.1038/ncomms15771

Takahashi, H., Su, H., & Jiang, J. H. (2016). Water vapor changes under global warming and the linkage to present-day interannual variabilities in CMIP5 models. *Climate Dynamics*, *47*(12), 3673–3691. https://doi.org/10.1007/s00382-016-3035-5

Taylor, K. E., Stouffer, R. J., & Meehl, G. A. (2012). An overview of CMIP5 and the experiment design. *Bulletin of the American Meteorological Society*, *93*(4), 485–498. https://doi.org/10.1175/BAMS-D-11-00094.1

Tian B., Manning, E., Fetzer, E. J., Olsen, E., & Sun, W. (2013). AIRS/AMSU/HSB Version 6 Level 3 Product User Guide. Retrieved from http://disc.sci.gsfc.nasa.gov/AIRS/documentation/v6_docs/v6releasedocs-1/V6_L3_User_Guide.pdf

Waters, J. W., Froidevaux, L., Harwood, R. S., Jarnot, R. F., Pickett, H. M., Read, W. G., … Walch, M. J. (2006). The Earth Observing System Microwave Limb Sounder (EOS MLS) on the Aura satellite. *IEEE Transactions on Geoscience and Remote Sensing*, *44*(5), 1075–1092. https://doi.org/10.1109/TGRS.2006.873771

Yue, Q., Kahn, B. H., Fetzer, E. J., Shreier, M., Wong, S., Chen, X., & Huang, X. (2016). Observation-based longwave cloud radiative kernels derived from the A-Train. *Journal of Climate*, *29*(6), 2023–2040. https://doi.org/10.1175/JCLI-D-15-0257.1

Zelinka, M. D., Klein, S. A., Taylor, K. E., Andrews, T., Webb, M. J., Gregory, J. M., & Forster, P. M. (2013). Contributions of different cloud types to feedbacks and rapid adjustment in CMIP5. *Journal of Climate*, *26*(14), 5007–5027. https://doi.org/10.1175/JCLI-D-1%2000555.1

Zhou, C., Zelinka, M. D., Dessler, A. E., & Klein, S. A. (2015). Relationship between cloud feedbacks in response to climate change and variability. *Geophysical Research Letters*, *42*, 10,463–10,469. https://doi.org/10.1002/2015GL066698